-RESEARCH PAPER-

International Journal of Mining and Geo-Engineering

IJMGE

IJMGE 56-4 (2022) 383-390

DOI: 10.22059/IJMGE.2022.287780.594822

Reservoir characterization and porosity classification using a probabilistic neural network (PNN) based on single and multi-smoothing parameters

Masood Lashkari Ahangarani [a], Saeed Mojeddifar [a, *], Mohsen Hemmati Chegeni [a]

[a] *Mining Engineering Department, Arak University of Technology, Arak, Iran.*

Article History:

Received: 24 August 2019.

Revised: 27 May 2022.

Accepted: 29 May 2022.

ABSTRACT

A probabilistic neural network (PNN) is a feed-forward neural network using a smoothing parameter. We used the PNN algorithm based on single and multi-smoothing parameters for multi-dimensional data classification. Using multi-smoothing parameters, we implemented an improved probabilistic neural network (PNN) to estimate the porosity distribution of a gas reservoir in the North Sea. Comparing the results of implementing smoothing parameters obtained from model-based optimization and particle swarm optimization (PSO) indicated the efficiency of PNN in characterizing the gas. Also, results showed that while the PSO algorithm was able to specify smoothing parameters with more precision, about 9%, it was very time-consuming. Finally, multi PNN based on PSO was applied to estimate the porosity distribution of the F3 reservoir. The results validated the main fracture or gas chimney of the F3 reservoir with higher porosity. Also, gas-bearing layers were highlighted by energy and similarity attributes.

Keywords: *Probabilistic neural network, Smoothing parameter, Model-based optimization, Particle swarm optimization.*

1. Introduction

The main concern of petroleum industries is to find the porosity distribution of a reservoir to determine the flow patterns. Also, accurate estimates of porosity are crucial to detect the hydrocarbon accumulations in a basin in order to decrease drilling risk. The measurement of the cored rocks recovered from the reservoir is the best procedure for porosity estimation in the laboratory. It is a time-consuming process therefore all wells in a typical oil or gas field are logged using various tools to measure petrophysical parameters such as porosity and density [1, 2]. Also, seismic data are often applied to specify the structure of reservoir bodies, but it is very difficult to estimate the porosity directly from seismic data. Past studies showed that inversion of seismic data into acoustic impedance (AI) is widely used in hydrocarbon exploration to estimate petrophysical properties. The acoustic impedance is commonly used for porosity estimation, mostly based on an empirical relationship between acoustic impedance and porosity [3]. For this reason, Schultz et al. [4] proposed the idea of using multiple seismic attributes to estimate log properties. After that, various data integration techniques such as neural networks were used to derive petrophysical properties directly from seismic attributes. Recently, a probabilistic neural network (PNN) has been considered for data classification in many research studies in different fields. PNN is used extensively in geoscience studies. Adeli et al [5] used the PNN method to predict southern California's earthquake magnitude as a classification problem. PNN was used to map the geological and geophysical data to find the Platinum group elements (PGM) potential in the Carajás Mineral Province of Brazil [6]. Patel et al. [7] used PNN to classify the extracted image features from limestone rock images to monitor the quality of limestones. In other fields, PNN was used in medical diagnosis and prediction [8-12], and also image pattern recognition and classification were done by PNN [13, 14, 15, 16, 17].

Petrophysical properties such as permeability, density, porosity, shale volume, and acoustic impedance are the most useful properties for reservoir characterization of oil and gas fields. Lim et al. [18] used the PNN to estimate the reservoir permeability in offshore Korea. Singh et al. [19] used PNN to estimate porosity from 3D seismic attributes in the Cambay basin in the west of India. Herrera et al. [20] extracted shale volume from Gamma-ray log data and classify them via the PNN method to recognize productive sands and their boundaries. The mentioned research shows the ability of the PNN algorithm in the branches of geosciences. Therefore, the present work attempts to investigate the application of the PNN algorithm in reservoir characterization and determines the porosity distribution of the hydrocarbon reservoir based on PNN. The PNN uses a generalized nonlinear regression approach for rock type classification purposes. The smoothing parameter σ, controls the width of each Gaussian function in the PNN method. Single and multi-PNN methods differ in their definition of smoothing parameters. The single PNN method conserves the smoothing parameter value for all their inputs, whereas it has different values for each input attribute in the multi PNN method [21]. The smoothing parameter is the term of probability density function (PDF) and its optimal value can provide the pattern layer of PNN for high accuracy classification [22] .Although many researchers use the single value smoothing parameter [23, 24], some of them have shown that separate σ's for each dimension, improves the PNN result accuracy [25, 26]. This work aims to compare the results of single PNN and multi PNN in estimating the porosity of the gas reservoir of the F3 block in the North Sea. The optimum value of smoothing parameters in a single PNN is obtained by cross-validation technique, while model-based optimization and particle swarm optimization (PSO) are chosen for finding the optimum values of smoothing parameters in multi PNN.

* Corresponding author: *E-mail address:* mojeddifar@arakut.ac.ir (S. Mojeddifar).

2. Probabilistic neural network (PNN)

Artificial neural network (ANN) is an architecture consisting of a large number of neurons organized in different layers and the neurons of one layer are connected to neurons of another layer by means of weights. ANN can be programmed to train, store, recognize and associatively retrieve patterns or database entries in order to solve optimization problems. Training is the process of updating a neural network by modifying its weights. During the training, the parameter of the network is optimized, and as a result of this, it undergoes a process of curve fitting. The output of the network is compared with the corresponding target value and the error is determined. The obtained error is then propagated in the backward direction to update the connecting weights of the neuron, the so-called backpropagation algorithm, to get a more accurate prediction. The major difference between a traditional ANN and PNN is related to the mechanism of learning and updating their weights. PNN was first introduced by Specht [27]. This network is a special type of radial basis function that is very faster than the back propagation algorithm [28]. The structure of PNN, as shown in Figure 1, consists of four layers: input layer, pattern layer, summation layer, and decision layer.

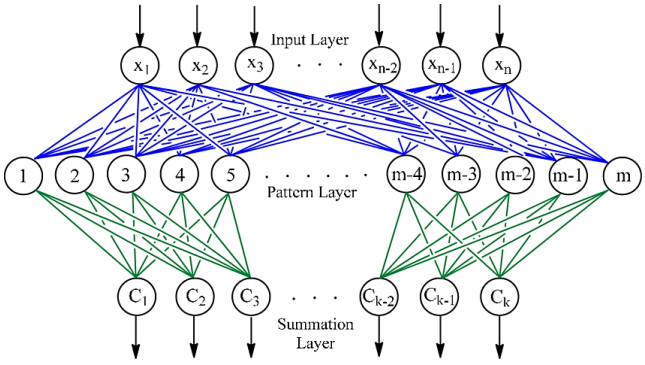

Figure 1. The general structure of the probabilistic neural network.

PNN is initially designed by using training samples for different classes. Then the probability value of the Gaussian function is calculated based on the distance of input data (the data with an unknown class) with each of the training samples in a special class, for example, *g*, using

$$Q_{ij} = \frac{1}{(2\pi)^{n/2}\sigma^n} \exp\left(-\frac{(x_j - x_{ij}^{(g)})^2}{2\sigma^2}\right) \quad (1)$$

where n is the dimension of the entries, and here, the number of attributes [28]. σ is the standard deviation of the Gaussian function that is equivalent to the smoothing parameter in PNN, $x_{ij}^{(g)}$ is the value of j-th attribute of the i-th training sample that belongs to the class g and x_j is the j-th attribute of the new input data [29]. Determining the class number of new input data is based on the results of Parzen window. Parzen window is:

$$p(x \mid c_g) = \frac{1}{(2\pi)^{\frac{n}{2}}\sigma^n} \frac{1}{l_g} \sum_{i=1}^{l_g} \exp\left(-\sum_{j=1}^{n} \frac{(x_j - x_{ij}^{(g)})^2}{2\sigma^2}\right) \quad (2)$$

The above equation is the mean of a probability distribution in input data (x_j) that combines all the training samples in each class ($x_{ij}^{(g)}$) for n attributes [22]. Here l_g is the number of training samples that belongs to class g. Parzen window's approach, introduced by Parzen [30] and developed by Cacoullos [31], estimates the class conditional probabilities as a sum of Gaussian kernel centered at the training points with appropriately chosen variances as equation 2. In equation 2, σ is the standard deviation of Gaussian kernels that play the role of smoothing parameter in Parzen window. It should be chosen based on the reasonable assumptions in order to increase Parzen's approach performance. Specht [27] suggested the cross-validation to estimate the smoothing parameter that the present research applied the cross-validation technique for the single PNN and discussed in the next sections.

The fourth layer of PNN determines the class of unknown input data with regard to the highest $p(x|c_g)$. Equation 2 shows that the only effective parameter is the smoothing parameter. For multi-smoothing parameterization, equation (2) evolves to:

$$p(x \mid c_g) = \frac{1}{(2\pi)^{n/2}\prod_{j=1}^{n}\sigma_j} \frac{1}{l_g} \sum_{i=1}^{l_g} \exp\left(-\sum_{j=1}^{n} \frac{(x_j - x_{ij}^{(g)})^2}{2\sigma_j^2}\right) \quad (3)$$

where σ_j is the smoothing parameter associated with the j-th attribute [32]. Finding the optimal value of the smoothing parameter is the most important challenge in a PNN algorithm. The particle swarm optimization (PSO) algorithm [33], Q-learning algorithm [32], and cross-validation [27] are some of the methods used to determine the optimum value of the smoothing parameter. Figure 2 shows the approach used in this paper based on cross-validation to find the optimum value of smoothing parameter for the single and multi PNN. Meanwhile, we applied a model-based optimization and a PSO optimization to estimate the optimum values of smoothing parameters for each input data in multi PNN.

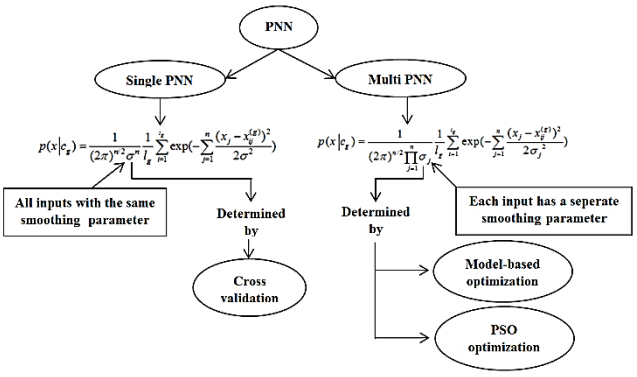

Figure 2. Diagram of determining smoothing parameter in single PNN and multi PNN.

3. Geological setting and data

The data used in this study was provided in F3 gas reservoir (Figure 3) by dGB Earth Science company. During the Cenozoic era, much of this region was a thermally subsiding epicontinental basin, most of which was confined by landmasses [34]. During the Neogene, sedimentation rates exceeded the subsidence rate and consequently shallowing of the basin occurred. A large fluvio-deltaic system dominated the basin, draining the Fennoscandian High and the Baltic Shield. The Cenozoic succession could be subdivided into two main packages, separated by the Mid-Miocene Unconformity. The lower package consists mainly of relatively fine-grained gradational Paleogene sediments [35], whereas the package above consists of coarser-grained Neogene sediments with much more complex geometries. Most of the above package is a progradational deltaic sequence that could be subdivided into three units, corresponding to three phases of delta evolution. The dominant direction of progradation is toward the west-southwest and is expressed as sigmoid lineaments (clinoforms) in the dip section [36]. Unit 2, containing a conspicuous clinoform package, was chosen as the target zone for gas accumulation, and forms the delta fore set with a coarsening upward sequence. Its age is estimated as Early Pliocene. The coarse sediments are attributed to a regression caused by the Neogene uplift of Scandinavia in the Pliocene [37]. Previous geological studies had shown that this reservoir consists of several sandstone sequences and shale layers. A sandstone layer is located between two shale formations. On the other hand, previous studies and obtained information from drilled wells show that the gas accumulation

was located in the sandstone layer [34]. A 3D seismic survey in F3 block has been provided publicly available by dGB Earth Science, and is prepared in a monograph by Aminzadeh and Groot [38]. Seismic attributes were calculated using OpendTect software and porosity values were extracted from the neutron log. Figure 3 displays four well in the study area.

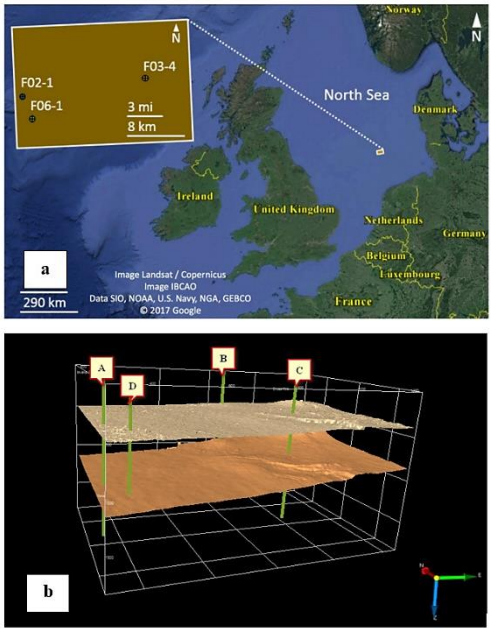

Figure 3. (a) Location of F3 block and available wells overlaid on a Google Earth image; (b) 3d view of F3 reservoir and location of drilled wells between two horizons.

Seismic attributes are used as inputs of single and multi PNN to determine the class of porosity as an output. Statistical studies of 8 attributes, computed by Opendtect software, were performed in this research. The list of the employed attributes and their correlation coefficients with porosity values are presented in Table 1.

According to Table 1, Similarity, Semblance, Energy, and Ins-Amplitude were chosen by correlation over 0.25. Effective attributes should have less correlation together than employed as nearly independent variables for estimating the porosity. Thus, Semblance was eliminated due to a high correlation (0.96) by Similarity. Then, three seismic attributes of energy, similarity, and instantaneous amplitude were selected due to the higher correlation with the porosity parameter than other attributes. The extracted data contains 800 samples and 161 samples were randomly selected as test data set. The seismic attributes are employed to classify the input data in 10 classes of porosity from 0.22 to 0.3 with step 0.008 in F3 block. The following is a brief explanation of the seismic attributes that select as inputs:

Similarity attribute which is the simplest coherence attribute is given by OpendTect dGB Plugins User Documentation [39]:

$$sim = 1 - \frac{\sqrt{\sum_{i=1}^{n} (x_i - y_i)^2}}{\sqrt{\sum_{i=1}^{n} x_i^2} + \sqrt{\sum_{i=1}^{n} y_i^2}} \quad (4)$$

Where sim is the similarity value calculated for the analyzed window including n number of data from x and y vectors. Term n usually is specified by seismic traces of the analyzed window. The numerator calculates the Euclidean distance for traces x and y in a time window and the sum of the vector's length is computed in the denominator. Similarity attribute is an index to identify the resemblance of seismic traces with each other. It means that the traces which are located in the same positions like faults or boundaries related to lithological changes are expected to show the same properties. Energy attribute is one of the main seismic attributes which is calculated by:

$$E(t, x, y, t_1, t_2) = \sum_{\tau=t_1}^{t_2} u(t+\tau, x, y)^2 \quad (5)$$

Where E(.)is the energy attribute; u(.)is the amplitude of the signal trace; τ is the time step in the analysis window. Energy attribute is known as an exploration tool to detect the bright spot anomaly in a gas-bearing reservoir.

The attribute of instantaneous amplitude is measured by the following formula:

$$a(t) = \sqrt{x(t)^2 + y(t)^2} \quad (6)$$

Where *x(t)* and *y(t)* represent the amplitude variations of seismic trace on the *X* axis and *Y* axis, respectively. The most important application of the instantaneous amplitude attribute is to study acoustic impedance changes and to detect the bright spot anomaly in a hydrocarbon reservoir.

4. Single PNN based on cross-validation

Seismic attributes of energy, similarity, and instantaneous amplitude are used as inputs of a single PNN algorithm to recognize the class of porosity as an output. A number of 639 data samples is applied to learn the single PNN and the value of the smoothing parameter is changed to classify correctly 161 test samples. Figure 4 shows the number of test samples which is correctly classified by the single PNN versus variation of the smoothing parameter. According to Figure 4, the best results are obtained by the single PNN when the smoothing parameter is equal to 0.06.

Figure 4. Illustration of different smoothing parameters of single PNN vs correct. pixels.

Table 1. Correlation coefficients of the used seismic attributes versus porosity log.

Seismic attributes	Porosity	Similarity	Semblance	Energy	Ins-Amplitude	Ins-Phase	Ins-Frequency	Ins-Hilbert	Ins-Q factor
Porosity	1	0.2932108	0.2764108	0.39418	0.256863137	0.0727141	0.17025539	0.11440451	0.091594927
Similarity	0.293211	1	0.96199626	0.46932	0.277026994	0.0877056	0.154268547	0.03581204	0.020967147
Semblance	0.174952	0.9534367	1	0.31196	0.154319727	0.1145717	0.151966091	0.08402292	0.042114429
Energy	0.394182	0.4693179	0.40991508	1	0.5849972	0.0731257	0.024669058	0.02662874	0.025812912
Ins-Amplitude	0.276863	0.277027	0.24602906	0.585	1	0.0805702	0.209198481	0.10086868	0.059421242
Ins-Phase	0.072714	0.0877056	0.09001831	0.07313	0.080570244	1	0.07660859	0.63898601	0.037969432
Ins-Frequency	0.170255	0.1542685	0.14022762	0.02467	0.209198481	0.0766086	1	0.04323455	0.059585528
Ins-Hilbert	0.114405	0.035812	0.04657246	0.02663	0.100868679	0.638986	0.043234552	1	0.068299334
Ins-Qfactor	0.091595	0.0209671	0.04796265	0.02581	0.059421242	0.0379694	0.059585528	0.06829933	1

5. Multi PNN

To determine the optimum values of smoothing parameters for each input separately, two techniques of model-based optimization and PSO algorithm were used. Here, we give a brief explanation of the two methods.

5.1. Multi PNN based on model-based optimization

Model-based optimization is initiated by the multivariate nonlinear regression model between the different smoothing parameters and the total number of correctly classified data as a dependent variable. This model was designed by changing the smoothing parameters independently, in the range [0.01, 0.2] with step 0.01. In each mode, PNN algorithm was implemented and 161 test data were evaluated to count the number of correctly classified pixels. The mathematical model was obtained by response surface analysis in MINITAB® software and is shown in equation (7).

$$CP=96.142 - 57.38X_1 + 29.56\,X_2 + 476.91\,X_3 - 205.6\,X_1^2 - 259.2\,X_2^2 - 1404.2\,X_3^2 - 15.6\,X_1X_2 - 374.2\,X_1X_3 - 186.0\,X_2\,X_3 \quad (7)$$

Where CP is the total number of correctly classified data, X_1 is the smoothing parameter of energy, X_2 is the smoothing parameter of similarity and X_3 is the smoothing parameter of instantaneous amplitude. The second-order model was selected because the second-order model is proper to extend the area of changes of the response variable by including the main effects, curvature, and interaction effects of independent variables as shown in equation (7).

5.2. Multi PNN based on PSO optimization

The PSO optimization algorithm first proposed by Kennedy and Eberhart [40], is another method used to optimize the values of multi-smoothing parameters. This algorithm initially produces n random particles in the search space and tries to optimize the target function by changing the position of these particles. Each particle has a velocity vector and a position vector that is generated in an iterative process using

$$v_{id}^{k+1} = v_{id}^{k} + c_1 r_1^{k}(pbest_{id}^{k} - x_{id}^{k}) + c_2 r_2^{k}(gbest_{d}^{k} - x_{id}^{k}) \quad (8)$$

$$x_{id}^{k+1} = x_{id}^{k} + v_{id}^{k+1} \quad (9)$$

where, r_1 and r_2 are random numbers between [0, 1] and c_1 and c_2 are constant coefficients. $X_i = (x_{i1}, x_{i2}, ..., x_{iD})$ represents i-th particle of the D-dimensional search space set and if the change in the position of the i-th particle leads to the improvement of the target function. The new X_i is shown with pbesti = $(p_{i1}, p_{i2}, ..., p_{iD})$; the best pbest is denoted by gbest. Finally, after k iteration, pbesti is the best personal experience for i-th particle and gbest is the best experience of the entire set [40]. The PSO algorithm in the present study is used to find optimum values of multi-smoothing parameters. Also, the number of particles in the search space (n) was 100 and the number of iterations in the algorithm (k) was 1000. The estimated optimum value of a single smoothing parameter and the optimum values of multi-smoothing parameters by model-based optimization and PSO algorithm and their corresponding correct points are compared in Table 2.

According to Table 2, the PSO algorithm classified 141 pixels correctly in comparison with model-based optimization. Although the PSO algorithm has higher accuracy than model-based optimization it took 24 hours to respond while it is a lot in comparison to just a few seconds of model-based optimization as an analytical method

6. Validation

After finding the optimum values of smoothing parameters in single and multi PNN (based on PSO and model-based optimization), a confusion matrix is employed to provide a more accurate estimate of the performance of developed algorithms. The confusion matrix is a matrix in which column i represents the data that belongs to the i-th class and the row j represents the data that is classified by the PNN algorithm on the j-th class. It is obvious that the pixels located on the main diameter indicate the data that is correctly placed in true classes by the algorithm. If the sum of the data in the main diameter is divided by the total sum of matrix data, the overall accuracy is obtained which indicates the algorithm's accuracy in classification. Table 3 shows the confusion matrix of a single PNN that was optimized by cross-validation technique and Table 4 shows the confusion matrix of multi PNN based on model-based optimization.

The comparison between Table 3 and Table 4 proves that multi-PNN could be used more accurately for porosity data classification in the gas reservoir. The reason is that the nature of seismic attributes is different with regard to their frequency distributions. The frequency distribution of energy, similarity, and instantaneous amplitude attributes is presented in Figure 5. Heterogeneity of these attributes causes less accuracy in single PNN in comparison to multi PNN. Single PNN is appropriate when attributes are homogeneous while the similarity attribute is a geometric attribute that indicates the spatial and temporal connection of a signal with its surrounding signals, and the instantaneous amplitude attribute offers a snapshot of a signal. Therefore, it is obvious that the nature of the input attributes is different and their distributions are different from each other significantly.

Table 2. Calculated smoothing parameters for single PNN and multi PNNs.

PNN Algorithm	Energy	Similarity	Ins-Amplitude	Correct pixels
Single PNN	0.06	0.06	0.06	112
Multi PNN with model-based optimization	0.010	0.012	0.168	127
Multi PNN with PSO optimization	0.0451	0.0379	0.2071	141

Table 3. Confusion matrix of single PNN developed by cross validation.

Single PNN	class1	class2	class3	class4	class5	class6	class7	class8	class9	class10	total	Commission Error
class1	**6**	2	0	0	0	1	0	1	0	0	10	0.4
class2	4	**4**	3	0	0	0	0	1	0	0	12	0.667
class3	0	4	**2**	1	0	1	0	1	0	0	9	0.556
class4	0	0	1	**8**	3	0	1	0	0	0	13	0.385
class5	0	1	0	0	**16**	3	0	2	0	0	22	0.273
class6	1	0	0	1	4	**24**	1	0	0	0	31	0.226
class7	0	0	0	0	0	2	**16**	4	0	0	22	0.273
class8	0	0	0	0	1	1	1	**28**	1	0	32	0.125
class9	0	0	0	0	0	0	0	2	**6**	0	8	0.25
class10	0	0	0	0	0	0	0	0	0	**2**	2	0
total	11	11	6	10	24	32	19	39	7	2	161	
Omission Error	0.45	0.64	0.67	0.2	0.3	0.25	0.2	0.3	0.1	0	**Overall accuracy: 0.695652**	

Table 4. Confusion matrix of multi PNN developed by model-based optimization.

Multi PNN: model based	class1	class2	class3	class4	class5	class6	class7	class8	class9	class10	total	Commission Error
class1	**7**	1	0	0	0	1	1	0	0	0	10	0.3
class2	3	**6**	1	0	0	0	0	1	0	0	11	0.454
class3	0	3	**4**	1	0	0	0	0	0	0	8	0.5
class4	0	0	1	**9**	1	0	0	0	0	0	11	0.182
class5	0	1	0	0	**18**	1	0	1	0	0	21	0.143
class6	1	0	0	0	5	**26**	0	0	0	0	32	0.187
class7	0	0	0	0	0	1	**16**	3	0	0	20	0.2
class8	0	0	0	0	0	0	2	**32**	0	0	34	0.059
class9	0	0	0	0	0	0	0	2	**7**	0	9	0.222
class10	0	0	0	0	0	3	0	0	0	**2**	5	0.6
total	11	11	6	10	24	32	19	39	7	2	161	
Omission Error	0.4	0.45	0.33	0.1	0.3	0.19	0.2	0.2	0	0	**Overall accuracy: 0.78882**	

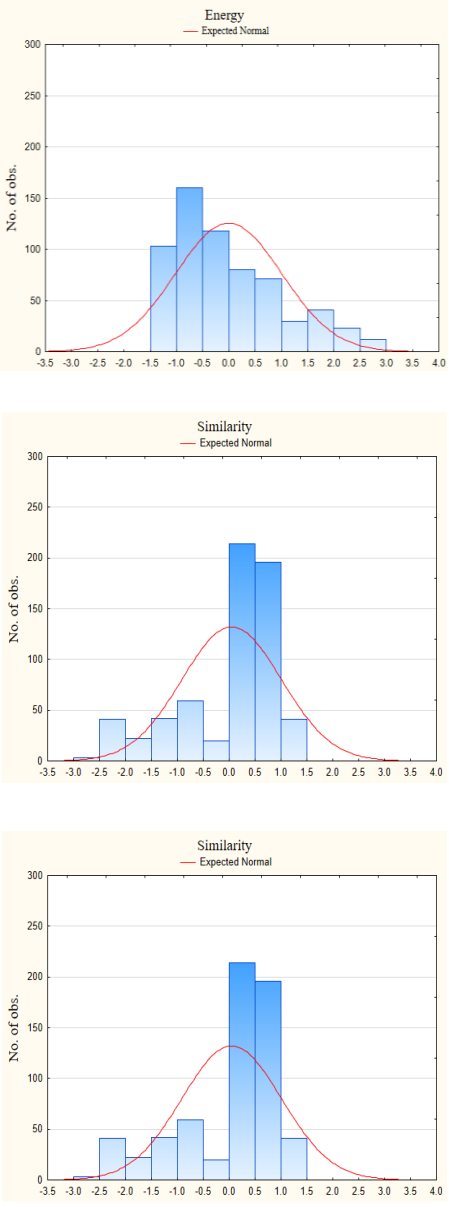

Figure 5. Frequency distribution of energy, similarity, and instantaneous amplitude attributes.

As shown in Table 4, multi-PNN is able to classify the test data in the correct classes with an accuracy of about 79%, which is acceptable performance. In order to evaluate more precisely the operation of the algorithm, commission error and omission error are defined were located in the last column and the last row of the confusion matrix, respectively. An omission error occurs when an area belongs to a class while it is estimated to be in a different class. A commission error occurs when an area is estimated to be in a class but does not belong to that class [41]. According to Table 4, the omission error for class 1 means that 40% of samples related to class 1 are classified in other classes incorrectly and the commission error for class 1 means that 30% of samples which belong to other classes were predicted in class 1 incorrectly. Table 5 presents the confusion matrix of multi-PNN based on the PSO algorithm. Based on Table 5, the overall accuracy is found to increase to 87%. Also, commission and omission errors have been significantly reduced. A comparison between Tables 4 and 5 indicates that the PSO algorithm is more accurate than the model-based optimization method for estimating the multi-smoothing parameters.

Validation showed that multi PNN based on PSO algorithm could present better results. Thus, it was used to classify the porosity distribution of F3 block in in-lines 244 and 336 as shown in Figure 6. Here, porosity has increased in the main fracture of the reservoir, shown with the ellipse. This fracture is known as a gas chimney in the F3 block and provides a way for gas to migrate from the Zechstein salt dome to above sand layers. On the other hand, it provides suitable space to accumulate gas. The rectangular polygon shows a gas-bearing sand layer that has been sandwiched between shale layers.

Main fractures and gas chimneys could be highlighted via the coherence attribute. The similarity is a simple kind of coherence that calculates the relationship between a central seismic trace and adjacent traces. Figure 7 shows the similarity attribute of F3 block in in-line 244. As illustrated with an ellipse, the main fracture of F3 block could be observed that it was classified with higher porosity values by multi PNN. Also, seismic attributes such as energy could prove the presence of gas in a reservoir. Energy attribute is a measure of changes in signal amplitude. It has been observed when seismic traces pass a gas-bearing zone, their amplitude change considerably. Therefore, the energy attribute identifies a gas presence anomaly, the so-called bright spot, (Figure 8). According to Figure 8, there is a bright spot anomaly in cross-line 900 located at top of the main fracture. It proves that the main fracture of F3 block contains gas accumulation.

7. Conclusion

The procedure of this study was focused on the statistical nature of seismic attributes because the performance of the PNN depends on its adjustable parameter which is called the smoothing parameter and the variation of seismic attributes as inputs determines the real smoothing parameter.

Table 5. Confusion matrix of multi PNN develop.

Multi PNN: model based	class1	class2	class3	class4	class5	class6	class7	class8	class9	class10	total	Commission Error
class1	**10**	1	0	0	0	0	0	0	0	0	11	0.091
class2	1	**7**	1	0	0	0	0	1	0	0	10	0.3
class3	0	3	**5**	0	0	0	0	1	0	0	9	0.444
class4	0	0	0	**10**	2	0	0	0	0	0	12	0.167
class5	0	0	0	0	**21**	3	0	1	0	0	25	0.16
class6	0	0	0	0	1	**29**	1	0	0	0	31	0.064
class7	0	0	0	0	0	0	**18**	3	0	0	21	0.143
class8	0	0	0	0	0	0	0	**32**	0	0	32	0
class9	0	0	0	0	0	0	0	1	**7**	0	8	0.125
class10	0	0	0	0	0	0	0	0	0	**2**	2	0
total	11	11	6	10	24	32	19	39	7	2	161	
Omission Error	0.09	0.36	0.17	0	0.1	0.09	0.1	0.2	0	0	**Overall accuracy: 0.875776**	

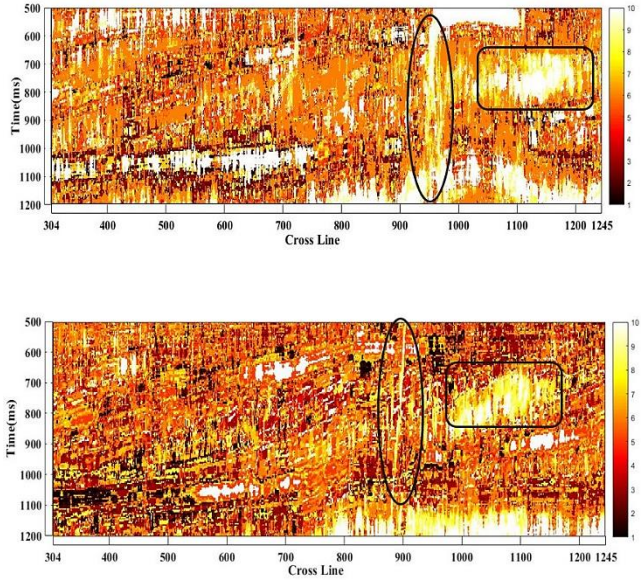

Figure 6. Porosity distribution in inline244 (A) and inline336 (B) by multi PNN based on PSO algorithm.

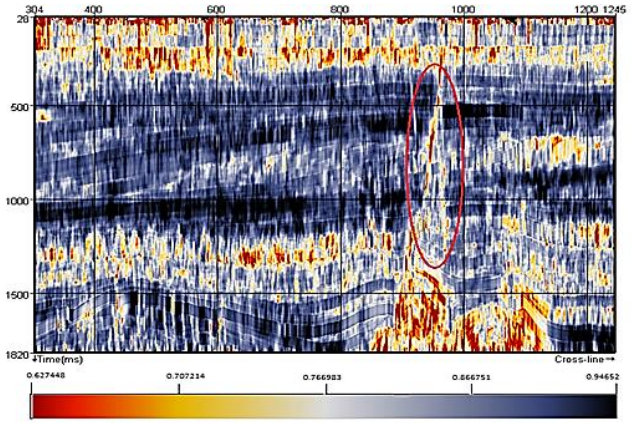

Figure 7. Similarity attribute in in-line 244.

Therefore, the same smoothing parameter for all seismic attributes is not a good idea hence the present work attempted to apply the multi-smoothing parameter PNN instead of one. PNN is able to determine the hidden relationships among the information extracted from the input data; this information can be trained with a set of responses and can be used to predict responses for unobserved samples. Different seismic attributes show different probability distributions and it means that the unique smoothing parameter could not address the hidden relationships. Also, the procedure of determining the smoothing parameter is another challenge of this research. Cross-validation, model-based optimization, and PSO optimization were considered to provide the appropriate PNN. Multi smoothing parameter PNN is more effective than single smoothing parameter PNN in the classification of data. A comparative study of model-based optimization and PSO algorithm was carried out to find the optimal values of smoothing parameters and the results showed that although the PSO algorithm is able to specify smoothing parameters with more precision, about 9%, it is very time-consuming. On the other hand, the accuracy provided by the model-based PNN (79%) is also acceptable and its operating speed is much faster than the PSO method, therefore the use of model-based optimization could be effective. Finally, multi PNN based on PSO was applied to estimate the porosity distribution of F3 reservoir. The results validated the main fracture or gas chimney of F3 reservoir with higher porosity. Also, gas-bearing layers were highlighted by energy and similarity attributes.

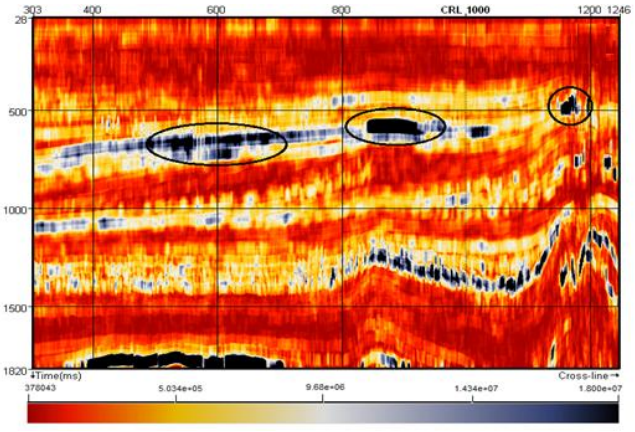

Figure 8. Energy attribute in in-line 244.

REFERENCES

[1] Bhatt A, Helle HB. Committee neural networks for porosity and permeability prediction from well logs. Geophys Prospect. 2002; 50:645–60.

[2] Tiab D, Donaldson EC. Petrophysics—theory and practice of measuring reservoir rock and fluid transport properties. 2nd ed. Melbourne: Elsevier; 2004.

[3] Anderson JK. Limitations of seismic inversion for porosity and pore fluid: lessons from chalk reservoir characterization

exploration. Denver: Society of Exploration Geophysicists, SEG Annual Meeting; 1996. p. 309–12.

[4] Schultz PS, Ronen S, Hattori M, Corbett C. Seismic-guided estimation of log properties (Part 1: a data-driven interpretation methodology). Lead Edge. 1994; 13:305–10.

[5] Adeli, H. and Panakkat, A. (2009). A probabilistic neural network for earthquake magnitude prediction. Neural networks. 22(7): p. 1018-1024.

[6] Leite, E.P. and de Souza Filho, C. R. (2009). Probabilistic neural networks applied to mineral potential mapping for platinum group elements in the Serra Leste region, Carajás Mineral Province, Brazil. Computers & Geosciences. 35(3): p. 675-687.

[7] Patel, A.K. and Chatterjee, S. (2016). Computer vision-based limestone rock-type classification using probabilistic neural network. Geoscience Frontiers. 7(1): p. 53-60.

[8] Er, O., et al. (2012) An approach based on probabilistic neural network for diagnosis of Mesothelioma's disease. Computers & Electrical Engineering. 38(1): p. 75-81.

[9] Huang, C.-J. and Liao, W.-C. (2003). A comparative study of feature selection methods for probabilistic neural networks in cancer classification. in Proceedings. 15th IEEE International Conference on Tools with Artificial Intelligence. IEEE.

[10] Mantzaris, D., Anastassopoulos, G. and Adamopoulos, A. (2011). Genetic algorithm pruning of probabilistic neural networks in medical disease estimation. Neural Networks, 24(8): p. 831-835.

[11] Shan, Y., et al. (2002). Application of probabilistic neural network in the clinical diagnosis of cancers based on clinical chemistry data. Analytica Chimica Acta. 471(1): p. 77-86.

[12] Gorunescu, F., et al. (2005). An evolutionary computational approach to probabilistic neural network with application to hepatic cancer diagnosis. in 18th IEEE Symposium on Computer-Based Medical Systems (CBMS'05). IEEE.

[13] Chtioui, Y., Bertrand, D. and Barba, D. (1996). Reduction of the size of the learning data in a probabilistic neural network by hierarchical clustering. Application to the discrimination of seeds by artificial vision. Chemometrics and Intelligent Laboratory Systems. 35(2): p. 175-186.

[14] Franti, P., et al. (2000). Fast and memory efficient implementation of the exact PNN. IEEE Transactions on Image Processing. 9(5): p. 773-777.

[15] Mohebian, R., Riahi, MA., Afjeh, M. (2018). Detection of the gas-bearing zone in a carbonate reservoir using multi-class relevance vector machines (RVM): comparison of its performance with SVM and PNN. Carbonates and Evaporites. 33, p. 347–357.

[16] Mohebian, R., Riahi, MA., Kadkhodaie, A. (2019). Characterization of hydraulic flow units from seismic attributes and well data based on a new fuzzy procedure using ANFIS and FCM algorithms, example from an Iranian carbonate reservoir. Carbonates Evaporites. 34, p. 349–358.

[17] Tofighi, F., Armani, P., Chehrazi, A., Alimoradi, A. (2021). Comparison of the Function of Conventional Neural Networks for Estimating Porosity in One of the Southeastern Iranian Oil Fields. Petroleum Research. 31, 118, 16-18.

[18] Lim, J.-S., Park, H.-J. and Kim, J. (2006). A new neural network approach to reservoir permeability estimation from well logs. in SPE Asia Pacific Oil & Gas Conference and Exhibition. Society of Petroleum Engineers.

[19] Singh, V., et al. (2007). Neural networks and their applications in lithostratigraphic interpretation of seismic data for reservoir characterization. The Leading Edge. 26(10): p. 1244-1260.

[20] Herrera, V.M., Russell, B. and Flores, A. (2006). Neural networks in reservoir characterization. The Leading Edge. 25(4): p. 402-411.

[21] Hampson, D.P., Schuelke, J.S. and Quirein, J.A. (2001). Use of multiattribute transforms to predict log properties from seismic data. Geophysics. 66(1): p. 220-236.

[22] Chettri, S.R. and Cromp, R.F. (1993). Probabilistic neural network architecture for high-speed classification of remotely sensed imagery. Telematics and Informatics. 10(3): p. 187-198.

[23] Mojeddifar, S., Chegeni, M.H. and Ahangarani, M.L. (2018). Gas-bearing reservoir characterization using an adjusted Parzen probabilistic network. Journal of Petroleum Science and Engineering. 169: p. 445-453.

[24] Kusy, M. and Kluska, J. (2013). Probabilistic neural network structure reduction for medical data classification. in International Conference on Artificial Intelligence and Soft Computing. Springer.

[25] Specht, D.F. and Romsdahl. H. (1994). Experience with adaptive probabilistic neural networks and adaptive general regression neural networks. in Proceedings of 1994 IEEE International Conference on Neural Networks (ICNN'94). IEEE.

[26] Farrokhrooz, M. and Karimi, M. (2007). A performance comparison between Conventional PNN and Multi-spread PNN in ship noise classification. in OCEANS 2006-Asia Pacific. IEEE.

[27] Specht, D.F. (1990). Probabilistic neural networks. Neural networks. 3(1): p. 109-118.

[28] El Emary, I.M. and Ramakrishnan, S. (2008). On the application of various probabilistic neural networks in solving different pattern classification problems. World Applied Sciences Journal. 4(6): p. 772-780.

[29] Mao, K.Z., Tan, K.-C. and Ser, W. (2000). Probabilistic neural-network structure determination for pattern classification. IEEE Transactions on neural networks. 11(4): p. 1009-1016.

[30] Parzen, E. (1962). "On estimation of a probability density function and mode." The annals of mathematical statistics 33(3): 1065-1076.

[31] Cacoullos, T. (1966). "Estimation of a multivariate density." Annals of the Institute of Statistical Mathematics 18(1): 179-189.

[32] Kusy, M. and Zajdel, R. (2014). Probabilistic neural network training procedure based on Q (0)-learning algorithm in medical data classification. Applied Intelligence. 41(3): p. 837-854.

[33] Georgiou, V.L., Alevizos, P.D. and Vrahatis, M.N. (2008). Novel approaches to probabilistic neural networks through bagging and evolutionary estimating of prior probabilities. Neural Processing Letters. 27(2): p. 153-162.

[34] Sørensen JC, Gregersen U, Breiner M, Michelsen O. High-frequency sequence stratigraphy of Upper Cenozoic deposits in the central and southeastern North Sea areas. Mar Pet Geol. 1997; 14:99–123.

[35] Steeghs P, Overeem I, Tigrek S. Seismic volume attribute analysis of the Cenozoic succession in the L08 block (Southern North Sea). Glob Planet Change. 2000; 27:245–62.

[36] Tigrek S. 3D seismic interpretation and attribute analysis of the L08 block, Southern North Sea Basin. M.S. thesis, Delft

University of Technology; 1988.

[37] Gregersen U. Sequence stratigraphic analysis of Upper Cenozoic deposits in the North Sea based on conventional and 3-D seismic data and well-logs. Ph.D. thesis, University of Aarhus; 1997.

[38] Aminzadeh, F. and De Groot, P. (2006). Neural networks and other soft computing techniques with applications in the oil industry: Eage Publications.

[39] OpendTectdGB Plugins User Documentation version 4.2. dGB Earth Sciences. Copyright 2002–2011. http://opendtect.org/rel/doc/ User/dgb/index.htm. Accessed 25 Aug 2012.

[40] Kennedy, J. and Eberhart, R. (1995). Particle swarm optimization (PSO). in Proc. IEEE International Conference on Neural Networks, Perth, Australia.

[41] Congalton, R.G. and Green, K. (2008). Assessing the accuracy of remotely sensed data: principles and practices: CRC press.